Metakaolin as a precursor of materials for applications in Cultural Heritage: geopolymer-based mortars with ornamental stone aggregates

Marina Clausi[1], Serena C. Tarantino[1,2*], Laura Lorenza Magnani[1], Maria Pia Riccardi[1], Cristina Tedeschi[3], Michele Zema[1,2]

[1]*Dipartimento di Scienze della Terra e dell'Ambiente, Università di Pavia, via Ferrata 9, I-27100 Pavia, Italy*

[2]*CNR-IGG, Sezione di Pavia, via Ferrata 9, I-27100 Pavia, Italy*

[3]*Dipartimento di Ingegneria Civile e Ambientale, Politecnico di Milano, Piazza Leonardo da Vinci 10, I-20133 Milano, Italy*

*Corresponding author. E-mail address: serenachiara.tarantino@unipv.it. Phone: +390382985876. Fax: +390382985890

E-mail addresses of authors: marina.clausi01@universitadipavia.it; serenachiara.tarantino@unipv.it; lauralorenza.magnani01@universitadipavia.it; mariapia.riccardi@unipv.it; cristina.tedeschi@polimi.it; michele.zema@unipv.it

Highlights

- High-grade kaolin is a good precursors of materials for use in Cultural Heritage
- High-strength MK-based geopolymers with high water/solid ratio are obtained at RT
- Such geopolymers are used as binders to prepare mortars with ornamental stones
- Mortars are mechanically and aesthetically compatible with original stones

Abstract

Potentialities and suitability of metakaolin-based geopolymers in Cultural Heritage have been explored. In particular, in order to evaluate their possible use as restoration materials in conservation of historic manufactures, mortars have been prepared by adding aggregates of Italian ornamental stones to alkali-activated metakaolin with binder/sand ratio of 1:1. To improve workability, geopolymer binders have been synthesized from metakaolin and sodium silicate solution with water/solid ratios between 0.33 and 0.66 and SiO_2/Al_2O_3 and Al_2O_3/Na_2O molar ratios of 3.70 and 1.04, respectively, and characterized by several techniques, including mechanical strength tests according to UNI EN 196-1. All binders display good mechanical properties, with compressive and flexural strength values as high as 72 MPa and 6 MPa, respectively, and decreasing with increasing water/solid ratio. The increase of water in geopolymer formulation has little negative effect on the aluminosilicate gel development and on the strength of these materials.

Mortars display a homogeneous and compact matrix, bonded (silicoaluminate aggregates) or interlocked (carbonate) with aggregates. Their compressive strengths fall in the masonry mortars class M20 range. Their pore size distribution guarantees good breathability and adaptability to the substrate. The final materials mimic the original stones, with good aesthetic compatibility.

Keywords: metakaolin; geopolymer; alkali silicates; Cultural Heritage

1. Introduction

Conservation practices make cultural heritage available to future generations. The maintenance of historic structures brings to the use of traditional materials and methods, but more and more frequently new ones are developed and proposed to safely preserve or restore monuments and artworks, including constructions manufactured in the last decades (Corradi et al., 2008; Valluzzi et al., 2014).

A new class of materials alternative to traditional binders, obtained by reaction of alkali with aluminosilicates, has been developed with a view towards reducing the CO_2 footprint of construction materials. Alkali activated materials (AAMs), including those called geopolymers, can exhibit a wide variety of properties and characteristics, depending on the raw material selection and processing conditions (Duxson et al., 2006; Provis, 2013; Provis and Bernal, 2014). They have therefore recently emerged as novel engineering materials with commercial and technological potential (Palomo et al., 2014; Van Deventer et al., 2012). They are prepared under mild processing conditions from inexpensive feedstocks, such as industrial wastes, like ground blast furnace slags and fly ashes, or calcined clays. Metakaolinite (MK), obtained by the calcination of kaolin clays, is considered to be a suitable precursor for geopolymer production due to its reactivity and predictable and tunable properties of the final geopolymer (Duxson et al., 2006; Siddique and Klaus, 2009). It has been shown that properties of geopolymers, such as high level of resistance to a range of different acids and salt solutions, low shrinkage and low thermal conductivity, are best achieved by MK-based geopolymers rather than fly ash-based ones (Duxson et al., 2007a; Palomo et al., 1992; Palomo et al., 1999). Exploitation of these properties will depend on the development of applications in which the relatively high cost of metakaolin compared to fly ash is not a driving consideration and in which a fairly pure and homogenous material is necessary. Cultural Heritage, in the authors' opinion, could be one of the contexts in which geopolymer-based binders prepared from high-grade metakaolin can find application and in which the abovementioned properties are of extreme importance.

Geopolymers have frequently been proposed as binder phases in mortars (Arellano-Aguilar et al., 2014; Kamseu et al., 2014; Pelisser et al., 2013; Vasconcelos et al., 2011), while very few applications in cultural heritage are reported in literature (Elert et al., 2008; Hanzlíček et al., 2009). Due to the large variability and different typologies of masonry structures included in our cultural heritage, a specific knowledge of both the materials to be repaired and the restoration materials is required. Experimental studies of the properties of retrofitting materials are indeed decisive to improve the knowledge of the whole restoration process. Mortars used in restoration practices should respect the requirements of compatibility with the original material from the chemical, physical and mechanical points of view, including showing similar aesthetic features (Van Balen et al., 2005; see also: ICOMOS/ISCARSAH Committee, Recommendations for the analysis, conservation and structural restoration of architectural heritage, 2005). In detail, their mechanical behaviour should guarantee good adhesion to the substrate and the ability to adapt themselves to the masonry movements, being softer than the original material (Gulotta et al., 2013b; Lanas and Alvarez-Galindo, 2003). Naturally, the great variability of historical buildings and structures needs a case-by-case approach, where the use of unconventional materials might result convenient.

In this work, mortars (the term is used here to generally indicate a mixture of binder and aggregates) have been synthesized by using MK-based geopolymers as binder phase. The effects of a fluid slurry on the mechanical strength, binding capacity and chemical properties of the products are investigated. The study has been organized as follows:

- a high-quality kaolin has been selected as starting material in order to i) respect the high standard requested in the field of restoration of cultural heritage structures, and ii) have a convenient ‘reference system’;
- geopolymer binders have been prepared with different water/solid ratios. Maturation has been carried out at room temperature in order to simulate an outdoor setting;
- physico-chemical characterization of binders has been carried out by Fourier Transform Infrared Spectroscopy in Attenuated Total Reflectance (FTIR-ATR), X-ray Powder

Diffraction (XRPD), Mercury Intrusion Porosimetry (MIP) and mechanical tests. Microstructural features and their variations with water/solid ratio have been analyzed in detail by Field Emission Scanning Electron Microscopy (FESEM) and discussed with respect to binding efficiency of geopolymer formulation;

- geopolymer-based mortars have been synthesized by using i) standard sand and ii) powders from two different ornamental stones as aggregates;
- the effect on the final product of including fine size fraction (< 63 μm) of ornamental stones aggregates has been evaluated from the aesthetic and physico-chemical viewpoints.

2. Materials and methods

2.1 Materials

A high-quality kaolin clay, labelled Sl-K and composed of 73 wt% kaolinite and 23 wt% quartz, was used as raw material. It was provided by Sibelco Italia S.p.A. and derives from the Seilitz kaolin deposits (Germany). More information about its chemical composition, particle size distribution and dehydroxylation kinetics were given by Gasparini et al. (2013). A study making use of this kaolin clay to produce geopolymers has been reported by Gasparini et al. (2015). The kaolin powder was submitted to thermal treatment at 800°C for 2 hours to obtain the reactive metakaolin, hereafter labelled Sl-MK, characterized by a specific surface area of 12.04(5) m^2/g, as measured by nitrogen adsorption BET analysis. Sodium silicate solution supplied by Ingessil s.r.l. (Na_2O 14.37 wt%, SiO_2 29.54 wt%, H_2O 56.09 wt%) and NaOH pellets (Sigma-Aldrich, purity ≥ 98%) were used.

For the preparation of geopolymer-based mortars (see par. 2.2.2), a standard siliceous natural sand conforming to norm UNI-EN 196-1:2005, provided by Société Nouvelle du Littoral, and crushed ornamental stones were used as aggregates. Two varieties of Italian stones, Pietra di Angera and Pietra Serena, mainly employed for decorative purposes, were selected. Pietra di Angera is a dolostone (yellow variety), and the sample used for this work comes from the collection

of the Department of Earth and Environment Sciences of University of Pavia. Pietra Serena, a sandstone characterized by low porosity and mainly composed of quartz, feldspars, micas and fragments of silicate and carbonatic rocks, was provided by Consorzio Pietra Serena of Firenzuola, Italy. Chemical compositions of these stones, determined by FESEM-EDAX energy dispersive spectrometry (EDS), are reported as oxides wt% in Table 2.

2.2 Sample preparation

2.2.1 Geopolymer binders

For the synthesis of geopolymer binders, the sodium silicate solution was modified by adding distilled water and dissolving solid sodium hydroxide; four different sodium silicate solutions were prepared with H_2O/Na_2O ranging between 10 and 20. Sl-MK was allowed to react with each of these solutions, in order to obtain, for all samples, the following molar ratios: $SiO_2/Al_2O_3 = 3.7$ and $Al_2O_3/Na_2O = 1.04$. In fact, a SiO_2/Al_2O_3 ratio of around 4 provides the MK-based geopolymers with the highest strength and without formation of crystalline zeolite-type phases, as reported in the literature (Duxson et al., 2005; Fletcher et al., 2005; Komnitsas and Zaharaki, 2007). In particular, SiO_2/Al_2O_3 ratio of 3.7 was selected in order to mature geopolymers at room temperature and obtain high values of mechanical resistance, as indicated by the compressive strength vs. composition contour plot reported in Fig 1 of Burciaga-Diaz et al. (2012). Different H_2O/Na_2O molar ratios were used with the aim of improving the slurry workability, and obtaining water/solid ratios between 0.33 and 0.66. Sample labels and water/solid ratios used for the synthesis are reported in Table 1.

Water/solid ratio is a variable that influences physical and mechanical behaviour of mortars and concrete. In case of concrete, compressive strength is inversely correlated to water/solid ratio through the Abrams' generalization law. Furthermore, a ratio between 0.30 and 0.40 reduces durability issues due to increasing of the porosity and development of hydration products (Aïtcin, 2003). In mortars, the increase of water content improves their workability, but eventually reduces

148 the strength of hardened products. It was observed that the minimum water/solid ratio required to
149 make a cement mortar workable is about 0.50 (Haach et al., 2011; Rao, 2001; Singh et al., 2015). In
150 geopolymer synthesis, water results to have great effects on the development of geopolymer gels
151 and on the properties of the final products. In terms of strength, the minimization of water/solid
152 ratio corresponds to an increase of compressive strength and to a reduction of permeability (Rashad,
153 2013; Van Deventer et al., 2012; Zhang et al., 2010).

154 Geopolymer binder samples were prepared by adding Sl-MK powder to the alkaline
155 solutions and mixing for 10 minutes to form homogenous slurries. Mixing operations were
156 performed by using a mechanical mixer, according to the European technical standard (UNI-EN
157 196-1:2005), under controlled conditions of temperature and relative humidity (20°C and 65%
158 R.H., respectively). Samples were poured into prismatic steel moulds (4 × 4 × 16 cm^3) and
159 compacted by mechanical vibration for 60s to remove entrained air. Specimens were cured in
160 climatic room for 28 days at 20°C and 65% R.H. before testing. Three specimens for each
161 geopolymer binder were prepared.

162

163 *2.2.2 Geopolymer-based mortars*

164 Three geopolymer-based mortars were prepared by mixing the geopolymer binder slurry
165 GpB_0.66 with, respectively, standard sand (StS_GpM) and powders obtained by grinding Pietra
166 Serena (PS_GpM) and Pietra di Angera (PA_GpM).

167 Mortars were prepared in compliance with the requirements of UNI-EN 196-1:2005, but for
168 StS_GpM, a binder/sand ratio of 1:2 (weight/weight) was used, thus giving a mortar with
169 water/solid ratio of 0.23, whereas for mortars with crushed ornamental stones, PS_GpM and
170 PA_GpM, a binder/aggregate ratio of 1:1 was used to obtain mortars with a water/solid ratio of
171 0.39. For these samples, the granulometric fraction smaller than 0.5 mm was used as aggregate in
172 the preparation of mortars. Clayey fractions were also included to make the colour tone of the
173 mortars similar to that of their respective stone.

Each paste was mixed for 10 minutes, poured into prismatic steel moulds (4 × 4 × 16 cm^3) and compacted by mechanical vibration for 60s. All samples were submitted to maturation phase in climatic room for 14 days at 20°C and 90% R.H., then were de-moulded and cured at the same conditions for other 14 days.

2.3 Sample Characterization

2.3.1 X-ray Powder Diffraction (XRPD)

XRPD analyses were carried out on all samples by using a Philips PW1800/10 X-ray diffractometer, equipped with a Cu anticathode and a graphite monochromator. Data were collected in the range 2-65° 2θ with an angular step of 0.01° 2θ and time per step of 5s.

2.3.2 Fourier Transform Infrared Spectroscopy in Attenuated Total Reflectance (FTIR-ATR)

FTIR-ATR spectra were collected at room temperature in the range of wavelength between 670 and 4000 cm^{-1} with 4 cm^{-1} resolution by means of a ThermoScientific Nicolet iN10 MX micro-spectrometer. Spectra, recorded in ATR with a liquid nitrogen-cooled mercury cadmium telluride array detector, were calculated by Fourier transformation of 256 interferometer scans and total scanning time of 90s. A germanium hemispherical internal reflection element (IRE) crystal with a diameter of 300 μm was used. The ATR accessory is mounted on the X-Y stage of the FTIR microscope, and the IRE crystal makes contact with the sample via a force level with pressure of 2 Pa. A 150 × 150 μm^2 aperture size was used. IR spectra were recorded on the surface of compressed powder pellets of geopolymer binders.

2.3.3 Thermogravimetric analysis (TGA)

TG analyses were performed by using a TA instruments Hi-Res Modulated TGA 2950 Termogravimetric Analyzer. 15 mg of finely ground powders of geopolymer binders were heated in

199 a Pt crucible at 10°C/min heating rate under nitrogen atmosphere in the temperature range 30-
200 1000°C.
201
202 *2.3.4 Field Emission Scanning Electron Microscopy (FESEM)*
203 A Field Emission Scanning Electron Microscope TESCAN Mira 3 XMU-series, equipped
204 with an EDAX energy dispersive spectrometer, was utilized to investigate samples textures from
205 micrometric to nanometric scale. Analyses of the morphological features were performed on
206 fracture surfaces of the specimens, obtained by placing thin splinters of material directly on the
207 stab. Samples were covered by 5 nm carbon coating before being investigated to prevent charge
208 built-up on electrically insulating sample surface. Images were collected using backscattered
209 electron (BSE) and secondary electron (SE) at a working distance of 15.8 mm with an acceleration
210 voltage of 20 kV and 30 kV. Microstructural observations at the nanometer scale were carried out
211 by InBeam mode using a working distance of 5 mm. EDS analyses (on spots and on areas of 25
212 μm^2) were done with accelerating voltage of 20 kV, working distance of 15.8 mm, beam current of
213 20 µA and spot diameter of about 5 µA, acquiring for 100s per spot analysis. Chemical
214 compositions were determined considering 100 wt% oxide content on an H_2O- and CO_2-free basis
215 and are reported in Table 2.
216
217 *2.3.5 Mercury intrusion porosimetry (MIP) and gas pycnometry*
218 A Micrometrics Autopore IV 9500 series mercury intrusion porosimeter was used to analyze
219 prismatic samples of approximately 1 × 2 × 2 cm^3. A pressure from 0.10 to 60000.00 psia was
220 applied. Results are reported in Tables 1 and 3 for binders and mortars, respectively.
221 Densities of mortars were measured by a ULTRAPYC 1200e gas ultrapycnometer
222 (Quantachrome Instruments, USA) and are reported in Table 3. Measurements were carried out in a
223 sample chamber of 48.1 cm^3 and using nitrogen as pycnometric gas. For each sample, density was

obtained by averaging six measurements. Data accuracy is < ±0.02% and reproducibility is < ±0.01%. Stainless-steel spheres were used for instrument calibration.

2.3.6 Mechanical tests

Flexural strengths of geopolymers and mortars cured for 28 days were measured by the three point bending mode on 4 × 4 × 16 cm^3 prismatic specimens. Compressive strengths were measured using a Controls press equipped with a 250 kN load cell on residual pieces obtained from flexural tests according to UNI-EN 196-1:2005 (Methods of testing cement – Part 1: Determination of strength; 2005). Data are reported in Tables 1 and 3 for binder and mortars, respectively.

2.3.7 Colorimetry

Colorimetric measurements of geopolymer-based mortars and original ornamental stones were carried out by a Konica Minolta CM-2600d instrument. A spot of 6 mm in diameter was used. For each sample, six measurements were performed on different areas of the external surface. Values are reported in Table 3 and are expressed in the CIELAB (L*,a*,b*) colour coordinates system, where L* defines lightness and ranges from 0 (total absorption or black) to +100 (white), whereas a* and b* denote the green/red and blue/yellow values, respectively, both ranging between -60 and 60.

3. Results

3.1 MK-based geopolymer binders

3.1.1 Structural properties

No significant differences in the diffraction patterns of geopolymer binders with different water content were observed. XRPD patterns of all samples show a broad hump between 20 and 35° 2θ, typical of the amorphous phase of geopolymers. The only crystalline phase revealed by XRPD is quartz, which derives from the kaolin precursor and remains stable up to about 1000°C. No peaks

250 associated with zeolite phases and soluble salts were detected. XRPD patterns are not reported here
251 being essentially featureless; however the pattern for GpB_0.66 is used for comparison with mortars
252 in par. 3.2.1.

253 As for XRPD, also FTIR-ATR spectra of powders of geopolymer binders show similar
254 features (Figure 1). A broad band centered at about 990 cm^{-1} (peak maxima calculated from first
255 and second derivatives of the IR signal are reported in Table 1) represents the fingerprint of the
256 aluminosilicate geopolymer phase and demonstrates the formation of the geopolymer network in all
257 samples, as reported in many studies (Irfan Khan et al., 2015; Lee and Van Deventer, 2003; Lee and
258 van Deventer, 2004). Peaks in this region are related to asymmetric stretching of the Si-O-T bonds,
259 where T is Al or Si in tetrahedral coordination. This band has been fitted by using three Lorentian
260 components: one for the aluminosilicate gel, one for metakaolinite and one for quartz. The fits,
261 carried out by using the Multipeak Fitting package of Igor Pro 6.37, converged for the 4
262 formulations with nearly flat residuals curves. Fitted positions of peaks from metakaolinite and
263 quartz are centered, respectively, at around 1050 and 1140 cm^{-1} for all samples, as expected. Peak
264 from the aluminosilicate gel is centered at 990 cm^{-1}, as reported in literature. It is worth noting that
265 the relative area of quartz peak is about 15% and constant for all samples, while relative areas of
266 peaks from gel and metakaolinite show, with changing water content, slight variations which are
267 opposite one to the other. From inset of Figure 1 and data in Table 1, it is evident how the relative
268 area of peak from gel represents the largest part of the main peak area, and it decreases slightly with
269 increasing the water content in the geopolymer formulation. This may be interpreted as implying
270 that there is a reduction in the actual amount of gel, and hence of reactivity, at high water/solid
271 ratio. However, geopolymer relative peak area is large at water/solid ratio of 0.66, thus implying
272 that the metakaolinite conversion is high, and likewise the gel binder amount.

273 No features due to the presence of new crystalline phases are evident in the spectra but small
274 bands at around 1400 cm^{-1} can be related to CO_3^{2-} stretching vibrations and thus reveal the
275 formation of sodium carbonates. Sodium carbonate formation can be due to an excess of Na^+

cations that are mobile within pore network and, as water evaporates, are brought onto the surface and can then react with atmospheric CO_2. Trona, $Na_3(HCO_3)(CO_3)\cdot 2H_2O$, and other sodium carbonates, such as thermonatrite, $Na_2CO_3\cdot H_2O$, have already been observed as efflorescence in geopolymers and, although they may sometimes coexist, the nature and extent of efflorescence is related to humidity conditions during curing (Criado et al., 2005; Krivenko and Kovalchuk, 2007; Xie and Kayali, 2014). No correlation between carbonate formation and water/solid ratio of geopolymers is noted. Samples have been cured in air-tight containers and carbonate peaks are not evident in spectra collected on the surface of the as-demoulded samples but start to appear ca. 4h after the samples are exposed to air. It must be noted that IR spectra have been measured in ATR mode with Ge crystal, which is very sensible to surface effects (calculated penetration depth at 45° and 1000 cm^{-1} is 0.65 μm). The amount of carbonates is very low and below XRPD detection limit, and the only evidence of their presence is given by these IR peaks. However, the presence of potentially harmful compounds, such as soluble salts, could influence the potential applicability of geopolymers in restoration and precautions have to be taken into account. In restoration practices, the development of soluble salts is a common issue and the possible formation of potential harmful products needs to be accurately investigated with respect to the substrates to be restored.

The presence of water in geopolymers is proved by the bands at around 3400 and 1640 cm^{-1}, related to OH asymmetric stretching and H-O-H bending vibrations of molecular water, respectively. Both bands, and in particular that ascribed to OH-stretching, are broad and indicate a large disorder of hydroxyl groups and water molecules. Further indications on the presence of water and hydroxyl groups are also inferred by TG analysis. All the geopolymers of this study show the TG pattern typically observed for MK-based geopolymers (Provis and Van Deventer, 2009). Weight loss due to dehydration of loose water begins above room temperature and continues up to 300°C, when the bulk of free water has evaporated. At this temperature the weight loss is of about 16-17% for all the samples, irrespective of the water/solid ratio used for the synthesis. In fact, the largest weight loss occurs below 200°C, as already observed in other studies (Barbosa and

MacKenzie, 2003; Duxson et al., 2007b; Kong et al., 2007). Above 300°C and up to 800°C there is a further weight loss, which increases slightly from 1.6% for GpB_0.33 to 3.2% for GpB_0.66. Weight loss in this temperature range is attributed to dehydroxylation of chemically bound water, therefore the observed differences might suggest a difference in the amount of hydroxyls linked to the geopolymer gel.

Porosity of geopolymer binders increases from 21.5% to 31.8% with increasing the water/solid ratio from 0.33 to 0.66, as reported in Table 1. All samples are characterized by mesoporosity, with median pore radius ranging between 0.0057 and 0.0076 μm.

3.1.2 Mechanical properties

The mean values of three tests for flexural strength and six tests for compressive strength are reported in Table 1 and plotted in Figure 2. High values of compressive strength, between 72 MPa and 59 MPa, were obtained, with compressive resistance decreasing linearly with increasing the water/solid ratio. These values are higher than those reported in UNI-EN 998-2:2010 for masonry mortars, but similar to those reported in UNI-EN 206-1:2006 for high performance concrete (C 60/75). Considering the absence of aggregates in geopolymers, samples with low water content, such as GpB_0.33, could be preferentially chosen for structural applications.

Flexural strength slightly decreases with increasing water with a maximum difference of 2.5 MPa between samples with 0.33 and 0.66 water/solid ratio, respectively. At the end of flexural strength tests, specimen section fractures appeared flat and orthogonal to traction direction, the same fracture mode found in ceramic materials. Flexural data are in accordance with those reported in literature for MK-based geopolymers. Kamseu et al. (2014) found similar values for samples enriched with different percentages of fine aggregates. Furthermore, it has been demonstrated that flexural strength of MK-based geopolymers subject to aggressive media shows little or no variation (Palomo et al., 1999). Reduction of mechanical strength values with increasing water/solid ratio

may be ascribed to the increase of porosity rather than to a reduction of MK conversion into geopolymer.

The increase in water content has also extended the setting time of the samples. GpB_0.33 hardened after one day, while 10 days were necessary for GpB_0.66. However after 28 days all specimens were suitably hardened to be used for mechanical tests.

3.1.3 Textural and microstructural properties

Differences in the morphology of the geopolymer binder matrices are hereafter analyzed based on high resolution SEM images at increasing magnifications. At low magnifications (500x and 5Kx) (Figure 3, left panel), the presence of porosity, porous size, matrix homogeneity and diffusion of micro-fractures network were taken into account. At 500x, the micrographs show, for all samples, a homogeneous and dense texture. In GpB_0.33, spherical pores of 50-70 micron in size are evident, whereas such porosity is not present in other samples. At this length scale, a textural feature common to all samples is the presence of micro-sized defects, such as micro-voids, which may be ascribable to entrapped air, and micro-cracks due to sample cutting and vacuum extraction during sample preparation. At 5Kx, the amorphous features are confirmed. No crystalline phases and few unreacted or partially reacted MK particles are found. The morphological features of the binder matrix show little difference among the samples: an articulated and rough surface is always evident, although the irregularities are at a shorter length scale for GpB_0.53 and GpB_0.66 samples.

Analyses at higher magnifications (50Kx to 150Kx) display clearly the differences in the microstructural features of geopolymer binders with different water/solid formulations (Figure 3, right panel). At this length scale, the distribution of grains, the rounding of the spherical particles, the development degree and the compaction mode were investigated. At 50Kx, it is evident how the matrix of sample GpB_0.33 shows a tendency to organize itself into parallel layers, a morphological feature related to MK. At higher magnification (150 Kx), concatenated spherical particles,

interconnected to create small clusters of aluminosilicate gel, become visible. The arrangement in parallel planes is still visible. Sample GpB_0.46 displays the same structural arrangement as GpB_0.33, with an increase in particle size. With increasing the water content (GpB_0.53 and GpB_0.66), particles become smaller than 50 nm and well confined into isolated elements. The matrix is made of ultra-fine particles, partially bonded together, and directionality disappears. An increase of matrix porosity is also evident, as confirmed by MIP measurements.

3.2 Geopolymer-based mortars

All geopolymer-based binders of this work show high mechanical strength, low porosity and relatively high amount of aluminosilicate binding phase. Therefore, the most fluid (and hence workable) formulation, i.e. GpB_0.66, was used to prepare mortars. These were prepared using different materials: a sandstone (Pietra Serena), a dolostone (Pietra di Angera) and standard sand. The latter was used to evaluate the binding capacity of the binder.

3.2.1 Structural properties

Diffraction patterns of mortars PS_GpM and PA_GpM are reported in Figure 4 and compared to those of GpB_0.66 and of original stones used as aggregates. For both samples, patterns show the peaks characteristics of quartz, deriving from the kaolin precursor, and of their respective aggregates, as expected. No efflorescence appears on mortar samples. XPRD analyses, performed after 90 days from mortars synthesis, confirmed the absence of any new crystalline phases. The presence of aggregates rich in aluminum (in PS_GpM) and calcium (in PA_GpM) could help reduce carbonate formation, producing an increase of crosslinking in the geopolymer binder and reducing the mobility of alkalis, as already noted by Najafi Kani et al. (2012).Densities of mortars, as measured by pycnometry (Table 3), are similar to those of their respective stones; this can be interpreted as a positive feature, if considering these materials for use in replacement

practices. Moreover, such values are of the same order of magnitude of those reported for MK-based geopolymers of composition Si/Al = 1.9 (Duxson et al., 2005).

Percent porosity of all mortars is nearly half that of the binder GpB_0.66, as expected (see data in Tables 1 and 3). However, while porosity of PA_GpM is similar to that of the "yellow" variety of Pietra di Angera, porosity of PS_GpM is higher than that of Pietra Serena (Cantisani et al., 2013; Fratini et al., 2014). Pore size distributions of all mortars fall in the mesoporosity range and are reported in Figure 5, where are compared with that of the geopolymer binder GpB_0.66. While the binder and the mortar with standard sand show almost unimodal distributions with a sharp main peak, mortars with ornamental stones show broad and multimodal distributions. In all three cases, the main peak in the differential curves of mortars is shifted towards larger pore size than in the binder, and there are additional pores, which are greater in size. Differences in pore size distribution of mortars are expected considering the differences in type, quantity, granulometric distribution as well as porosity of aggregates themselves.

Differential curve for mortar StS_GpM, prepared with standard sand, exhibits a sharply defined peak in the 0.004 to 0.015 μm range, indicating a nearly unimodal distribution of pore sizes. The presence of a sharply defined intrusion peak in the differential curve indicates the intrusion of mercury throughout a pore network connected to the specimen surface. Therefore, the main intrusion peak observed here corresponds to the minimum throat dimension of an interconnected capillary network.

In the other two mortars, the main band is large, displays many features and is centered at larger pore dimensions than StS_GpM. A second, more rounded peak appears at a larger pore size. In fact, the whole granulometric fraction smaller than 0.5 mm was used for the synthesis of PA_GpM and PS_GpM, including the fine size fraction (< 63 μm) of the crushed rock. This favours binder compaction in the mortars and reduces the amount of low-size pores if compared to the standard mortar Sts_GpM. Differential and cumulative intrusion curves for PA_GpM and PS_GpM clearly reveal how the global porosity is the result of the contribution of the porosity of both

aggregates and geopolymer binder. In PS_GpM, the pore size distribution below 0.032 μm displays features similar to those generally observed for different varieties of Pietra Serena sandstone (Cantisani et al., 2013; Fratini et al., 2014; Manganelli Del Fa, 1987). The same effect can be observed for the pore size distribution of PA_GpM, moreover, for this mortar, porosity of Pietra di Angera itself can contribute further to the porosity in the range between 0.1 and 1 μm (Soggetti and Zezza, 1983). The second rounded peak in the differential curve is usually attributed to larger pores present in the interfacial zone between aggregate and binder paste. In the differential curve of PA_GpM, this is more pronounced and broader than in the other two mortars, thus reflecting on the one side the aforementioned contribution of aggregates, but also a less linked interface between geopolymer gel and carbonate aggregates. Conversely, such porosity is reduced in StS_GpM and PS_GpM due to the reaction of geopolymer with siliceous aggregates.

A large porosity range distribution is particularly relevant in conservation issues in outdoor environments (e.g., Gulotta et al., 2013a). The low percentage porosity associated to large median pore radius of geopolymer-based mortars could be considered as a positive feature for possible restoration applications. Although this may not reduce or inhibit the decay of the original stone, it could offer better breathability and adaptability of mortar to the original substrate.

3.2.2 Mechanical properties

The results of mechanical tests on geopolymer-based mortars are reported in Table 3. No shrinkage of the gel during the curing was observed for all samples.

For StS_GpM, a compressive strength of 75(2) MPa was measured, comparable to the value obtained for the geopolymer binder GpB_0.33. This result encourages considering the use of a slight high amount of water rather than of plasticizers to improve fluidity and workability of a binder in restoration applications. With the use of plasticizers, Pacheco-Torgal et al. (2011) obtained compressive strength values of up to 50 MPa. The flexural strength is higher compared to geopolymer binders. The average value of 9(1) MPa confirms how the addition of aggregates favors

a decrease of fragility of the final product, which could bring benefits if used as retrofitting material. Observed flexural/compressive strength ratio of StS_GpM is similar to those reported for Pietra Serena and Pietra di Angera (Cantisani et al., 2013; Fiumara et al., 1979; Soggetti and Zezza, 1983).

PS_GpM and PA_GpM show compressive strength lower than StS_GpM, but in agreement with those recommended in UNI-EN 998-2:2010 for the masonry mortars class M20. The mechanical tests results can be explained by considering the morphology (low sphericity grains) of aggregates and that fine powders have also be used. In detail, for PA_GpM, deleterious effect on strength of adding significant percentages (> 20%) of alkaline earth carbonate minerals was already reported by Yip et al. (2008). For PS_GpM the fine aluminosilicate powders admixtures may play part in the geopolimerisation process, for example they may change local Al/Si ratio. The formation of nanometric neogenic crystals, which may have influenced the mechanical strength, has been observed by high magnification SEM (see par. 3.2.3). Although the negative effect on mechanical properties, these findings suggest further studies on the use of Pietra Serena itself as precursor in the synthesis of geopolymers.

3.2.3 Textural and microstructural properties

Mortar StS_GpM (Figure 6) has a quite compact microstructure, only few micro-fractures are observed within the mortar matrix or along the aggregates rims, likely due to cutting of the specimens for metallographic preparation. At high magnifications, the binder phase appears more homogeneous and compact if compared to that of the naked binder GpB_0.66. The spherical particles that compose the matrix show a particle size between 50 and 0.5 nm with a sub-rounded or rounded shape. The compaction of the mortar binder and its lower porosity with respect to the naked binder are due to the presence of aggregates.

In PS_GpM sample (Figure 7), aggregates are poorly sorted, as expected considering that powders have not be sieved, and are characterized by low sphericity grains, with an angular or sub

angular shape. A more detailed analysis of microstructure of quartz and feldspar grains evidences an incipient dissolution; boundaries of these siliceous minerals show embayments at a few micron length scale. At the interaction zone with the matrix, mica rims are sharp and regular. Few needle-shaped crystals are observed in this sample. Their small crystal size made EDS analyses impossible; however, on the basis of their morphology, these crystals could be attributed to framework silicates zeolites or feldspathoids. It could be hypothesized that such neogenic crystals may be due to the fine size fraction of Pietra Serena, which supplies soluble silico-aluminate phases. The availability of aluminum and silicon in solution may alter the Si/Al ratio on a local scale thus promoting zeolite crystallization.

PA_GpM (Figure 8) shows a network of micro-cracks in the binder matrix and along binder-aggregate interfaces. Cracks follow a preferential orientation starting from the grain rims and continuing in the binder with a radial trend. The particles size is poorly sorted, with a size ranging from coarse to very fine. The aggregates shape is from sub-angular to sub-rounded, with uneven rims with indentations where the binder phase fills the primary porosity. No microstructures associated with dissolution processes are observed. The boundary between aggregates and binder is sharp and well defined and follows grains irregularities. No structures characteristic of C–S–H gel are observed. However, EDX analyses indicate Ca and Mg uptake of geopolymer gel around aggregates particles. Likely, Ca and Mg concentrations remain low enough to avoid the formation of C-S-H, as indicated by Yip et al. (2008).

3.2.4 Aesthetic compatibility

Mortars PS_GpM and PA_GpM, prepared with powders of Pietra Serena and Pietra di Angera as mineral admixtures, may find application as decoration mortars or as sealing and repairing mortars for small gaps in masonries and stone artifacts. For these puroposes, their aesthetic features should be similar to those of the original stone. Rock fines have been added to homogeneously color the resulting mortar and colorimetric measurements performed. The average

of six measurements of L*,a*,b* space for each sample is reported in Table 3. As expected, diluting rock powders into a white matrix results in a solid with nearly the same color hue and paler than the original rock. Difference in color hue angle, $h_{ab} = \tan^{-1}(b^*/a^*)$, is less than 1 for PA_GpM and about 4 for PS_GpM. The main differences are due to lightness ΔL^* and color saturation ΔC^*, which is −4.9 and −1.9 for PA_GpM, and PS_GpM, respectively. The color variation between stone references and mortars has been evaluated by using the total color difference, expressed as $\Delta E = \mathrm{sqrt}[(L^*_1-L^*_2)^2+(a^*_1-a^*_2)^2+(b^*_1-b^*_2)^2]$. In both cases, the difference in visual appearance of the samples is small, being $\Delta E = 5$ and 11 for PA_GpM and PS_GpM, respectively, but however distinguishable by human eye. These results confirm the purpose to obtain recognizable materials.

4. Conclusions

Geopolymers are promising materials with potential use in many application fields, in particular as high performance, environmental-friendly materials for structural applications and possible replacement for ordinary Portland cement. However, Cultural Heritage is one additional field in which MK-based geopolymers may find application, thanks to their high durability and versatile range of physical properties that may possibly be tailored to guarantee functional and aesthetic compatibilities with the remnants of original materials.

Geopolymers have been obtained after consolidation of a fluid slurry without the use of plasticizers and additives and resulted to be largely composed by amorphous binding material and showed high strength and low porosity. The presence of aggregates from ornamental stones, namely Pietra Serena and Pietra di Angera, resulted in a reduction of strength, which however falls in the masonry mortars class M20. This may open the way to use them as sacrificial material for restoration of stone objects, as compatibility depends on the support features, hence mechanical compatibility should be adjusted to each particular case also in function of the destination of use. In these mortars, microfines seem to contribute to further reduce carbonate formation, which is however low. An increase of compaction and reduction of porosity of the matrix with respect to the

plain binder has also been observed, pore size distribution of the mortars are similar to those of the used ornamental stones, thus suggesting the possibility to tune breathability of the mortars by adjusting their formulation. Functional compatibility means not to damage the old masonry and in second place to be able to protect it against external actions. Water is one of the most effective destruction agents for old masonry: water transport, dissolution and transport of salts, but also biological colonization are issues to take into consideration and further studies are in hand to better evaluate them.

Finally, the use of rock fines allows to obtain materials that mimic the stone, thus reaching good aesthetic compatibility. In particular, mortars of the same color of the rock but slightly paler have been obtained. In restoration practice, this would allow to obtain materials that are recognizable, albeit similar, to the original substrate.

In the quest of designing new, high-performance materials that meet the requirements of sustainability and compatibility with the artifacts, this study shows good potentialities of geopolymer-based materials for uses in Cultural Heritage.

Acknowledgements. The authors wish to thank Sibelco Italia S.p.A., Ingessil s.r.l. and Consorzio Pietra Serena of Firenzuola for kindly providing the materials. Prof. Massimo Setti is kindly acknowledged for collection of XRPD patterns and Dr. Lorenzo Appolonia (Soprintendenza per i Beni e le Attività Culturali, Regione Autonoma Valle d'Aosta, Italy) for fruitful discussions.

References

Aïtcin, P.C., 2003. The durability characteristics of high performance concrete: a review. Cement and Concrete Composites 25, 409-420.

Arellano-Aguilar, R., Burciaga-Díaz, O., Gorokhovsky, A., Escalante-García, J.I., 2014. Geopolymer mortars based on a low grade metakaolin: Effects of the chemical

composition, temperature and aggregate:binder ratio. Construction and Building Materials 50, 642-648.

Barbosa, V.F.F., MacKenzie, K.J.D., 2003. Thermal behaviour of inorganic geopolymers and composites derived from sodium polysialate. Materials Research Bulletin 38, 319-331.

Burciaga-Diaz, O., Escalante-Garcia, J.I., Gorokhovsky, A., 2012. Geopolymers based on a coarse low-purity kaolin mineral: Mechanical strength as a function of the chemical composition and temperature. Cement and Concrete Composites 34, 18-24.

Cantisani, E., Garzonio, C.A., Ricci, M., Vettori, S., 2013. Relationships between the petrographical, physical and mechanical properties of some Italian sandstones. International Journal of Rock Mechanics and Mining Sciences 60, 321-332.

Corradi, M., Tedeschi, C., Binda, L., Borri, A., 2008. Experimental evaluation of shear and compression strength of masonry wall before and after reinforcement: Deep repointing. Construction and Building Materials 22, 463-472.

Criado, M., Palomo, A., Fernández-Jiménez, A., 2005. Alkali activation of fly ashes. Part 1: Effect of curing conditions on the carbonation of the reaction products. Fuel 84, 2048-2054.

Duxson, P., Provis, J.L., Lukey, G.C., Mallicoat, S.W., Kriven, W.M., Van Deventer, J.S.J., 2005. Understanding the relationship between geopolymer composition, microstructure and mechanical properties. Colloids and Surfaces A: Physicochemical and Engineering Aspects 269, 47-58.

Duxson, P., Fernández-Jiménez, A., Provis, J.L., Lukey, G.C., Palomo, A., van Deventer, J.S.J., 2006. Geopolymer technology: the current state of the art. Journal of Materials Science 42, 2917-2933.

Duxson, P., Provis, J.L., Lukey, G.C., van Deventer, J.S.J., 2007a. The role of inorganic polymer technology in the development of ‘green concrete’. Cement and Concrete Research 37, 1590-1597.

Duxson, P., Lukey, G.C., van Deventer, J.S.J., 2007b. Physical evolution of Na-geopolymer derived from metakaolin up to 1000°C. Journal of Materials Science 42, 3044-3054.

Elert, K., Sebastián, E., Valverde, I., Rodriguez-Navarro, C., 2008. Alkaline treatment of clay minerals from the Alhambra Formation: Implications for the conservation of earthen architecture. Applied Clay Science 39, 122-132.

Fiumara, A., Riganti, V., Veniale, F., Zezza, U., 1979. (On the preservation treatments of the Angera stone). Geologia Applicata e Idrogeologia 14, 191-214.

Fletcher, R.A., MacKenzie, K.J.D., Nicholson, C.L., Shimada, S., 2005. The composition range of aluminosilicate geopolymers. Journal of the European Ceramic Society 25, 1471-1477.

Fratini, F., Pecchioni, E., Cantisani, E., Rescic, S., Vettori, S., 2014. Pietra Serena: the stone of the Renaissance. Geological Society, London, Special Publications 407, 173-186.

Gasparini, E., Tarantino, S.C., Conti, M., Biesuz, R., Ghigna, P., Auricchio, F., Riccardi, M.P., Zema, M., 2015. Geopolymers from low-T activated kaolin: Implications for the use of alunite-bearing raw materials. Applied Clay Science 114, 530-539.

Gasparini, E., Tarantino, S.C., Ghigna, P., Riccardi, M.P., Cedillo-González, E.I., Siligardi, C., Zema, M., 2013. Thermal dehydroxylation of kaolinite under isothermal conditions. Applied Clay Science 80-81, 417-425.

Gulotta, D., Bertoldi, M., Bortolotto, S., Fermo, P., Piazzalunga, A., Toniolo, L., 2013a. The Angera stone: A challenging conservation issue in the polluted environment of Milan (Italy). Environmental Earth Sciences 69, 1085-1094.

Gulotta, D., Goidanich, S., Tedeschi, C., Nijland, T.G., Toniolo, L., 2013b. Commercial NHL-containing mortars for the preservation of historical architecture. Part 1: Compositional and mechanical characterisation. Construction and Building Materials 38, 31-42.

Haach, V.G., Vasconcelos, G., Lourenço, P.B., 2011. Influence of aggregates grading and water/cement ratio in workability and hardened properties of mortars. Construction and Building Materials 25, 2980-2987.

584 Hanzlíček, T., Steinerová, M., Straka, P., Perná, I., Siegl, P., Švarcová, T., 2009. Reinforcement of
585 the terracotta sculpture by geopolymer composite. Materials & Design 30, 3229-3234.
586 Irfan Khan, M., Azizli, K., Sufian, S., Man, Z., 2015. Sodium silicate-free geopolymers as coating
587 materials: Effects of Na/Al and water/solid ratios on adhesion strength. Ceramics
588 International 41, 2794-2805.
589 Kamseu, E., Cannio, M., Obonyo, E.A., Tobias, F., Bignozzi, M.C., Sglavo, V.M., Leonelli, C.,
590 2014. Metakaolin-based inorganic polymer composite: Effects of fine aggregate
591 composition and structure on porosity evolution, microstructure and mechanical properties.
592 Cement and Concrete Composites 53, 258-269.
593 Komnitsas, K., Zaharaki, D., 2007. Geopolymerisation: A review and prospects for the minerals
594 industry. Minerals Engineering 20, 1261-1277.
595 Kong, D.L.Y., Sanjayan, J.G., Sagoe-Crentsil, K., 2007. Factors affecting the performance of
596 metakaolin geopolymers exposed to elevated temperatures. Journal of Materials Science
597 43, 824-831.
598 Krivenko, P.V., Kovalchuk, G.Y., 2007. Directed synthesis of alkaline aluminosilicate minerals in a
599 geocement matrix. Journal of Materials Science 42, 2944-2952.
600 Lanas, J., Alvarez-Galindo, J.I., 2003. Masonry repair lime-based mortars: factors affecting the
601 mechanical behavior. Cement and Concrete Research 33, 1867-1876.
602 Lee, W.K.W., Van Deventer, J.S.J., 2003. Use of infrared spectroscopy to study geopolymerization
603 of heterogeneous amorphous aluminosilicates. Langmuir 19, 8726-8734.
604 Lee, W.K.W., van Deventer, J.S.J., 2004. The interface between natural siliceous aggregates and
605 geopolymers. Cement and Concrete Research 34, 195-206.
606 Manganelli Del Fa, C., 1987. Pietra serena e pietraforte: le arenarie utilizzate nell'architettura
607 fiorentina. Alterazione, restauro, conservazione, Il progetto di restauro e alcune
608 realizzazioni. Edizioni kappa, pp. 108-115.

609 Najafi Kani, E., Allahverdi, A., Provis, J.L., 2012. Efflorescence control in geopolymer binders
610 based on natural pozzolan. Cement and Concrete Composites 34, 25-33.
611 Pacheco-Torgal, F., Moura, D., Ding, Y., Jalali, S., 2011. Composition, strength and workability of
612 alkali-activated metakaolin based mortars. Construction and Building Materials 25, 3732-
613 3745.
614 Palomo, A., Glasser, P.F., 1992. Chemically-bonded cementitious materials based on metakaolin.
615 Institute of Materials, London, ROYAUME-UNI.
616 Palomo, A., Blanco-Varela, M.T., Granizo, M.L., Puertas, F., Vazquez, T., Grutzeck, M.W., 1999.
617 Chemical stability of cementitious materials based on metakaolin. Cement and Concrete
618 Research 29, 997-1004.
619 Palomo, A., Krivenko, P., Garcia-Lodeiro, I., Kavalerova, E., Maltseva, O., Fernández-Jiménez, A.,
620 2014. A review on alkaline activation: New analytical perspectives. Materiales de
621 Construcción 64.
622 Pelisser, F., Guerrino, E.L., Menger, M., Michel, M.D., Labrincha, J.A., 2013. Micromechanical
623 characterization of metakaolin-based geopolymers. Construction and Building Materials
624 49, 547-553.
625 Provis, J.L., 2013. Geopolymers and other alkali activated materials: why, how, and what?
626 Materials and Structures 47, 11-25.
627 Provis, J.L., Bernal, S.A., 2014. Geopolymers and Related Alkali-Activated Materials. Annual
628 Review of Materials Research 44, 299-327.
629 Provis, J.L., Van Deventer, J.S.J., 2009. Geopolymers: Structures, processing, properties and
630 industrial applications.
631 Rao, G.A., 2001. Generalization of Abrams' law for cement mortars. Cement and Concrete
632 Research 31, 495-502.
633 Rashad, A.M., 2013. Alkali-activated metakaolin: A short guide for civil Engineer – An overview.
634 Construction and Building Materials 41, 751-765.

635 Siddique, R., Klaus, J., 2009. Influence of metakaolin on the properties of mortar and concrete: A
636 review. Applied Clay Science 43, 392-400.
637 Singh, S.B., Munjal, P., Thammishetti, N., 2015. Role of water/cement ratio on strength
638 development of cement mortar. Journal of Building Engineering 4, 94-100.
639 Soggetti, F., Zezza, U., 1983. Possibility of exploitation and technical properties of the Angera
640 stone, Lago Maggiore. Geologia Applicata e Idrogeologia 18, 81-93.
641 Valluzzi, M.R., Modena, C., de Felice, G., 2014. Current practice and open issues in strengthening
642 historical buildings with composites. Materials and Structures 47, 1971-1985.
643 Van Balen, K., Papayianni, I., Van Hees, R., Binda, L., Waldum, A., 2005. Introduction to
644 requirements for and functions and properties of repair mortars. Materials and Structures
645 38, 781-785.
646 Van Deventer, J.S.J., Provis, J.L., Duxson, P., 2012. Technical and commercial progress in the
647 adoption of geopolymer cement. Minerals Engineering 29, 89-104.
648 Vasconcelos, E., Fernandes, S., Barroso de Aguiar, J.L., Pacheco-Torgal, F., 2011. Concrete
649 retrofitting using metakaolin geopolymer mortars and CFRP. Construction and Building
650 Materials 25, 3213-3221.
651 Xie, J., Kayali, O., 2014. Effect of initial water content and curing moisture conditions on the
652 development of fly ash-based geopolymers in heat and ambient temperature. Construction
653 and Building Materials 67, 20-28.
654 Yip, C.K., Provis, J.L., Lukey, G.C., van Deventer, J.S.J., 2008. Carbonate mineral addition to
655 metakaolin-based geopolymers. Cement and Concrete Composites 30, 979-985.
656 Zhang, Z., Yao, X., Zhu, H., 2010. Potential application of geopolymers as protection coatings for
657 marine concreteI. Basic properties. Applied Clay Science 49, 1-6.
658

Figure captions

Figure 1. FTIR spectra of geopolymer binders between 675 and 4000 cm^{-1}. In the inset: relative peak area of aluminosilicate gel as a function of the water/solid ratio.

Figure 2. (a) Compressive strength and (b) flexural strength of geopolymer binders as a function of the water/solid ratio.

Figure 3. FESEM micrographs of geopolymer binders with different water/solid ratios at different magnifications. Left panel: 500x (left); 5Kx (right). Right panel: 50Kx (left); 150Kx (right).

Figure 4. XRPD patterns of geopolymer mortars (red) and respective ornamental stones used as aggregates (black). XRPD pattern of geopolymer binder GpB_0.66 (blue) is also reported for comparison. Dol = Dolomite; Kfp = K-feldspar; Ms = Muscovite; Qtz = Quartz.

Figure 5. Pore distributions in geopolymer-based mortars as determined by MIP. Dotted line: StS_GpM; dot-dashed line: PS_GpM; dashed line: PA_GpM. Pore distribution in geopolymer binder GpB_0.66 is reported for comparison as solid line and refers to the right axis.

Figure 6. FESEM micrographs of geopolymer-based mortar StS_GpM at different magnification. In the inset: quartz grain included in matrix (magnification of 2.5Kx).

Figure 7. FESEM micrographs of geopolymer-based mortar PS_GpM at different magnifications.

Figure 8. FESEM micrographs of geopolymer-based mortar PA_GpM at different magnifications.

Table 1
Click here to download Table: Table 1.docx

Table 1. Details of geopolymer binders

Sample	H_2O/Na_2O ratio	water/solid ratio	Si-O-T (cm^{-1})[a]	Relative peak area[a]	Compressive strength (MPa)	Flexural strength (MPa)	Porosity (%)	Median pore radius (µm)	Mass loss (%)[b]
GpB_0.33	10	0.33	986	0.69(5)	72(3)	6.1(8)	21.5	0.0057	18
GpB_0.46	14	0.46	979	0.68(5)	66(4)	4.9(1)	24.3	0.0052	19
GpB_0.53	16	0.53	990	0.67(5)	63(8)	4.9(7)	29.8	0.0064	19
GpB_0.66	20	0.66	987	0.63(5)	59(4)	3.6(5)	31.8	0.0076	20

Standard deviations are in parentheses.

[a]From FTIR spectroscopy. Si-O-T peak position is calculated from the first and second derivatives of the IR line. Relative peak area is calculated from the areas of the fitted Lorentian components of the main IR band as the ratio between the area of the Lorentian curve centred at 990 cm^{-1} and the area of the whole band (standard deviation from the fit).

[b]From TG analysis.

Table 2. Chemical compositions (wt%) of Pietra di Angera and Pietra Serena.

Oxides	Pietra di Angera	Pietra Serena
MgO	33(2)	6.3(6)
CaO	64(2)	5(1)
SiO_2	0.8(2)	59(1)
FeO	2.2(1)	6.2(5)
Al_2O_3		16(1)
Na_2O		2.9(7)
K_2O		2.7(7)
SO_3		0.5(2)
TiO_2		1.4(4)
Total	100(1)	100(1)

Standard deviations are in parentheses.

Table 3
Click here to download Table: Table 3.docx

Table 3. Details of geopolymer mortars and ornamental stones used as aggregates.

Sample	Compressive strength (MPa)	Flexural strength (MPa)	Porosity (%)	Median pore radius (μm)	Density (g/cm^3)	Colorimetric CIELAB coordinates		
						L*	a*	b*
Sts_GpM	75(2)	9(1)	17.3	0.0090	2.419(5)	-	-	-
PA_GpM	18(5)	3.2(9)	17.8	0.0254	2.767(7)	81.3(4)	6.1(5)	22(1)
PS_GpM	21(3)	3.6(8)	14.1	0.0243	2.962(1)	73(1)	-0.07(1)	3.9(4)
Pietra di Angera	-	-	-	-	2.706(5)	80.2(7)	7.2(1)	26.4(6)
Pietra Serena	-	-	-	-	2.941(1)	62.2(7)	-0.45(5)	5.5(1)

Standard deviations are in parentheses.

Figure 1

Click here to download high resolution image

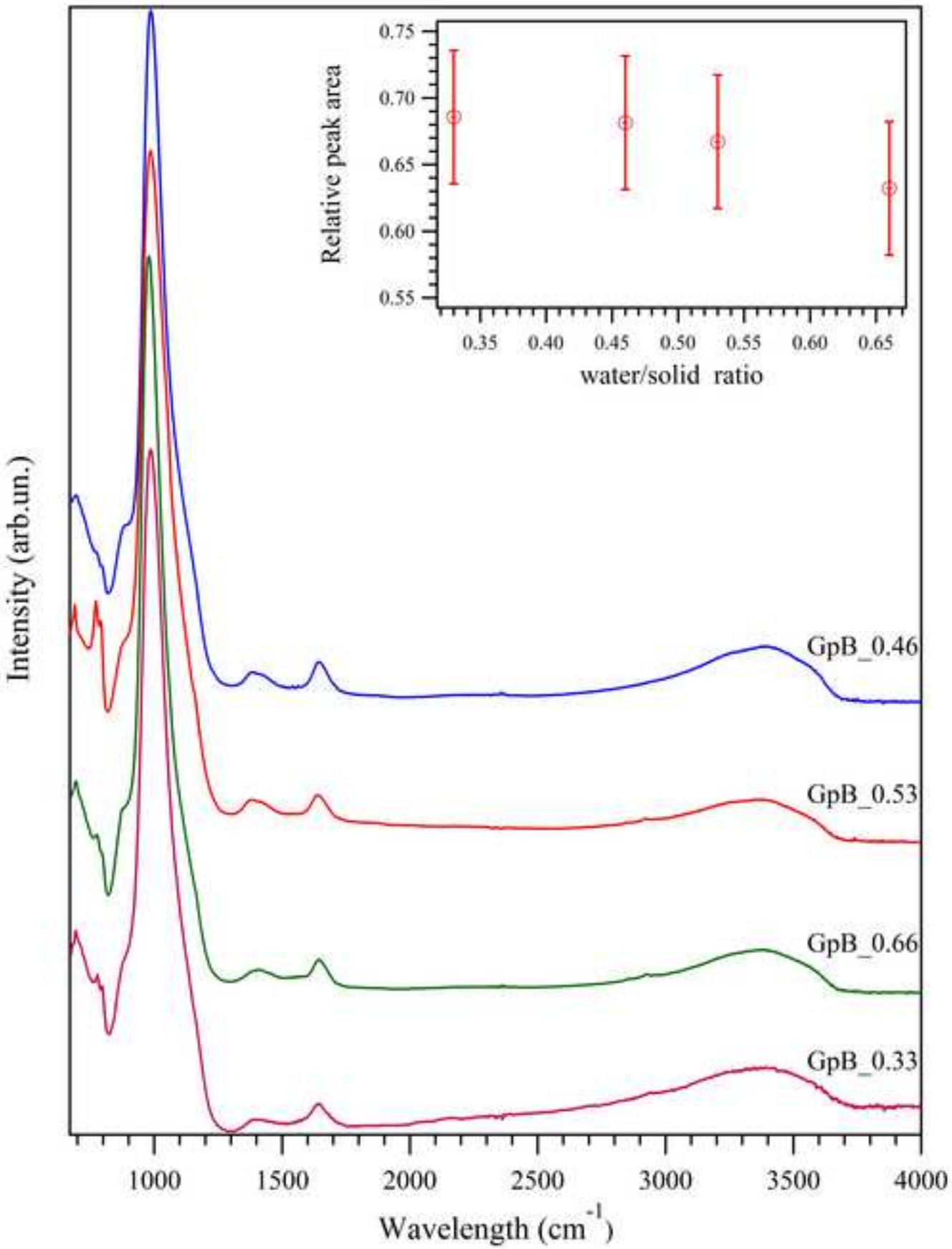

Figure 2
Click here to download high resolution image

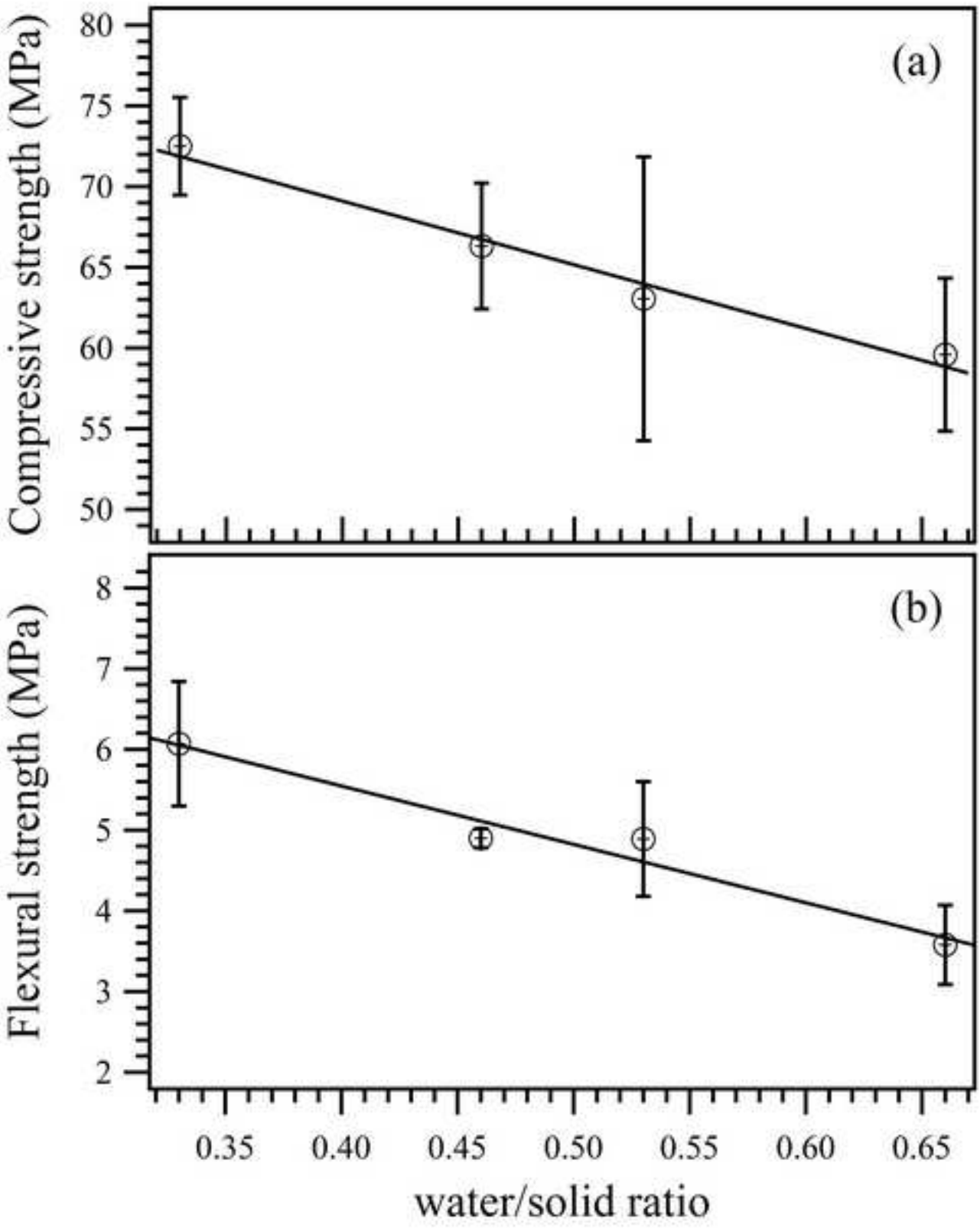

Figure 3 - Left panel

Click here to download high resolution image

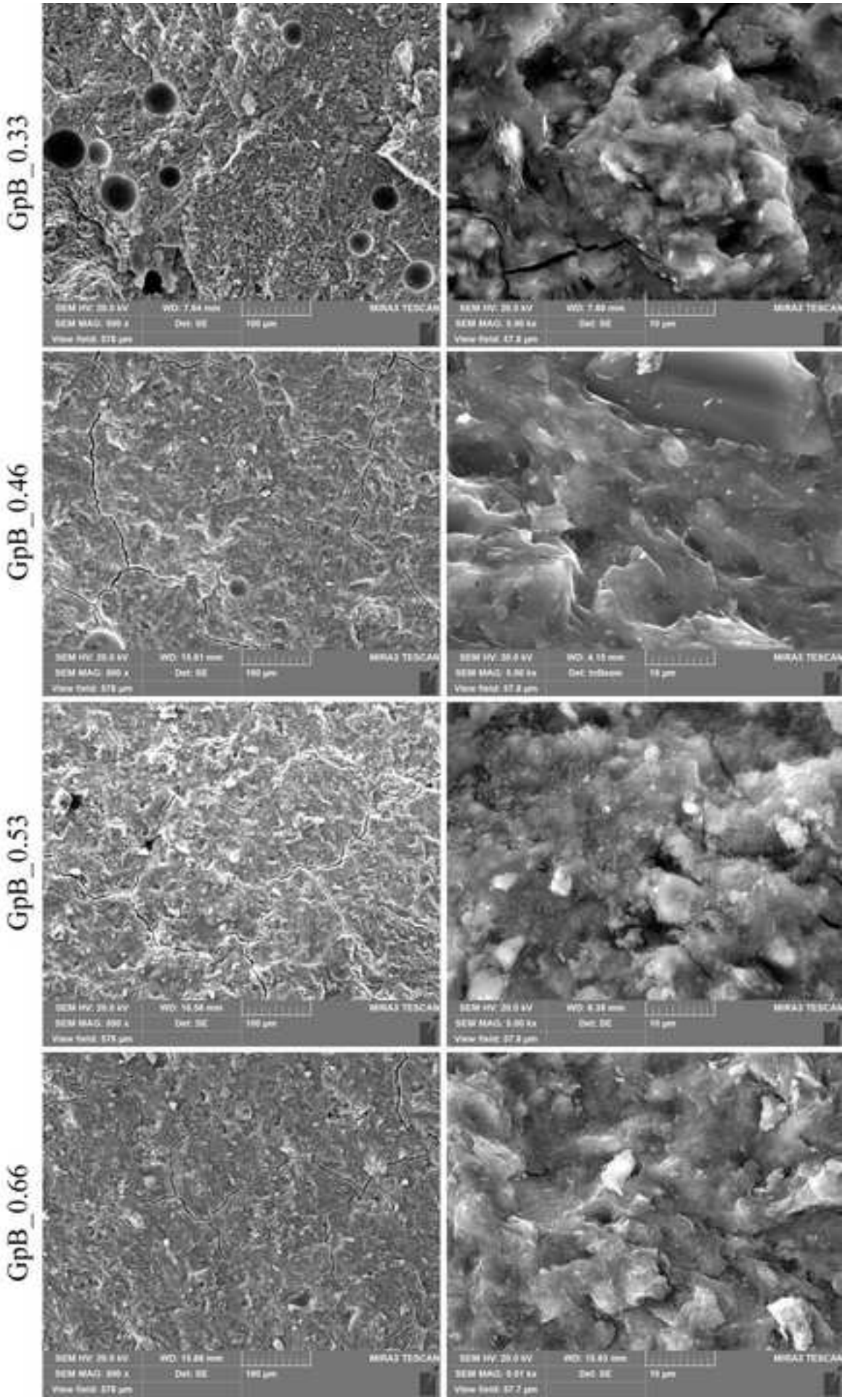

Figure 3 - Right panel

Click here to download high resolution image

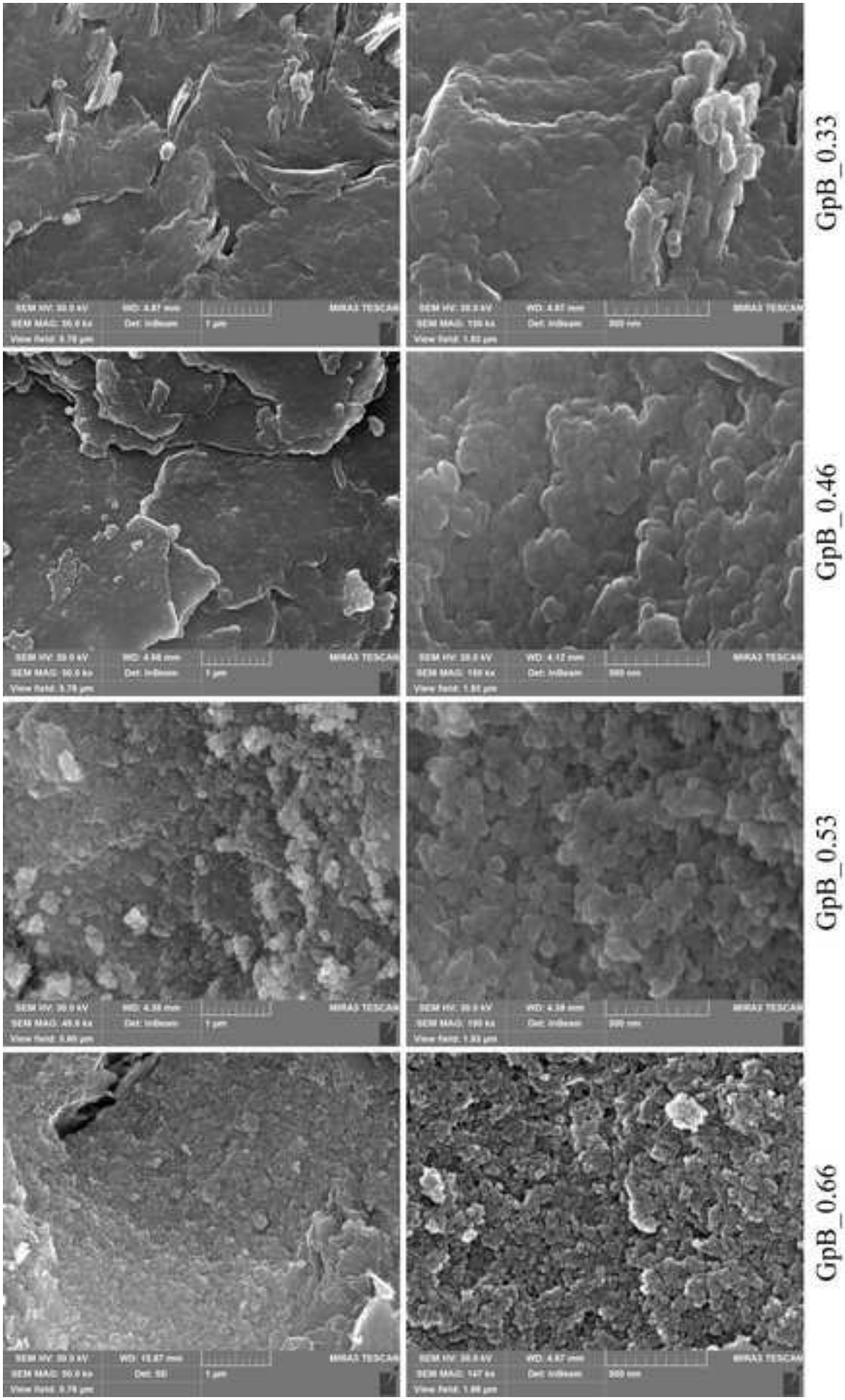

Figure 4

Click here to download high resolution image

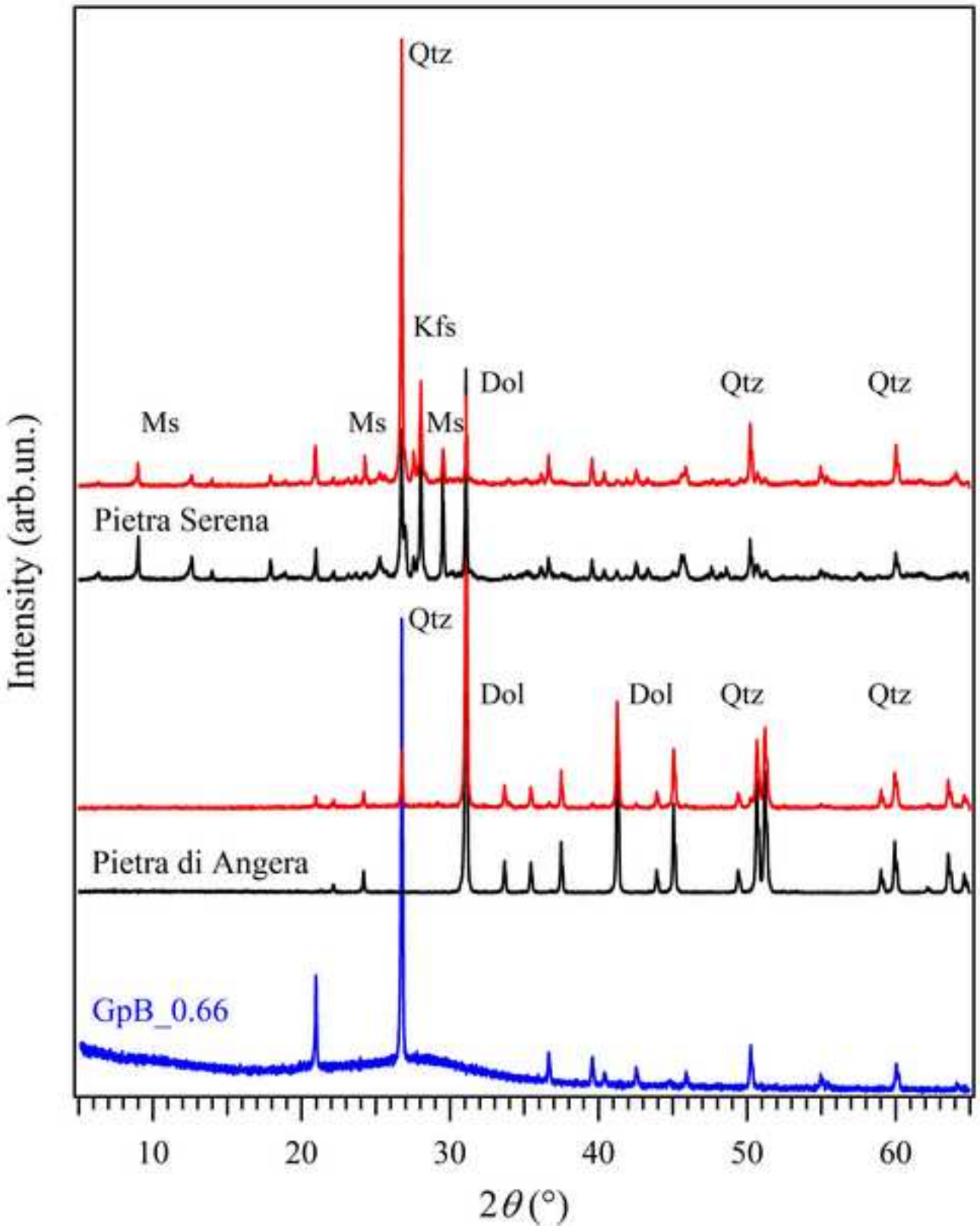

Figure 5

Click here to download high resolution image

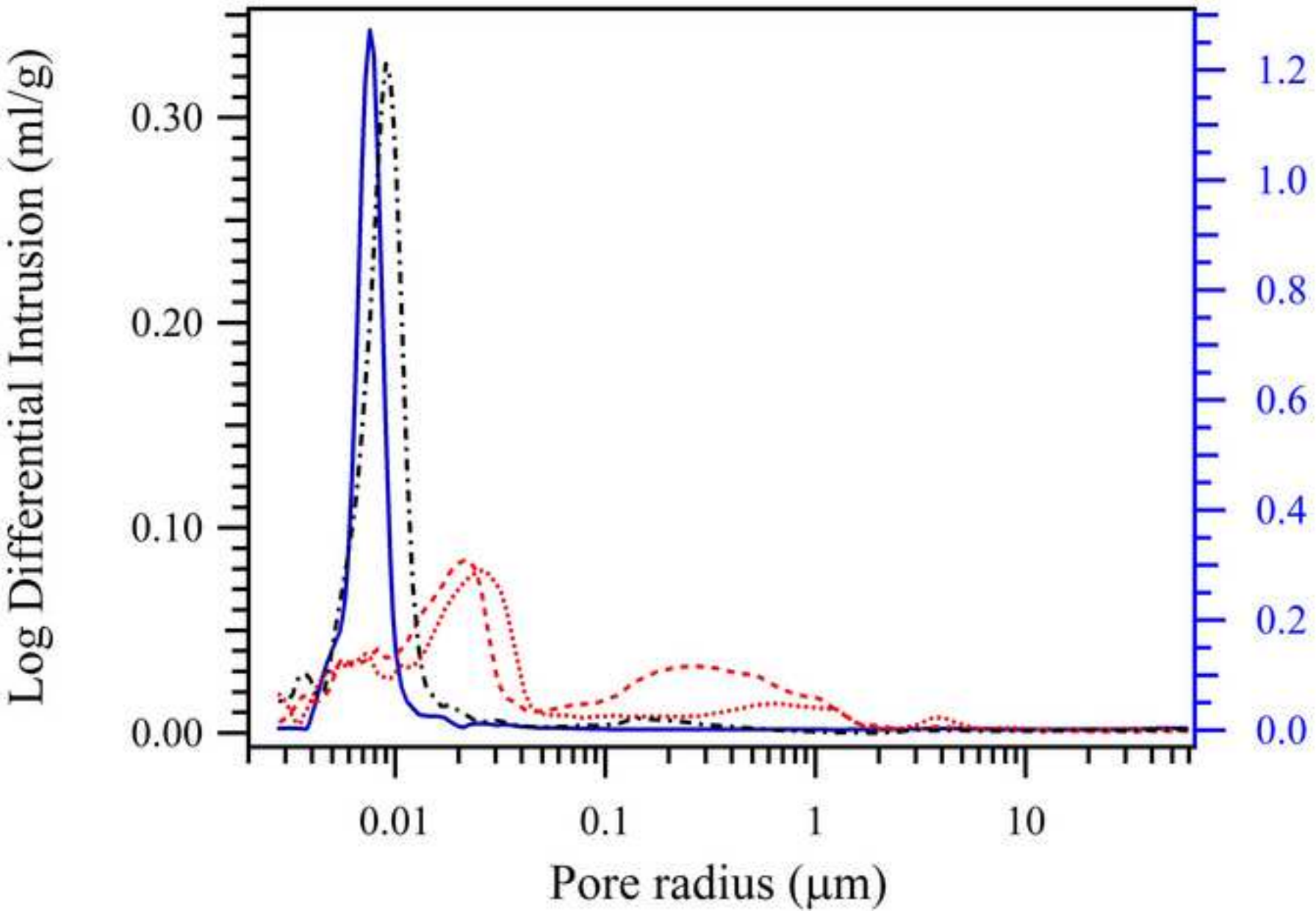

Figure 6

Click here to download high resolution image

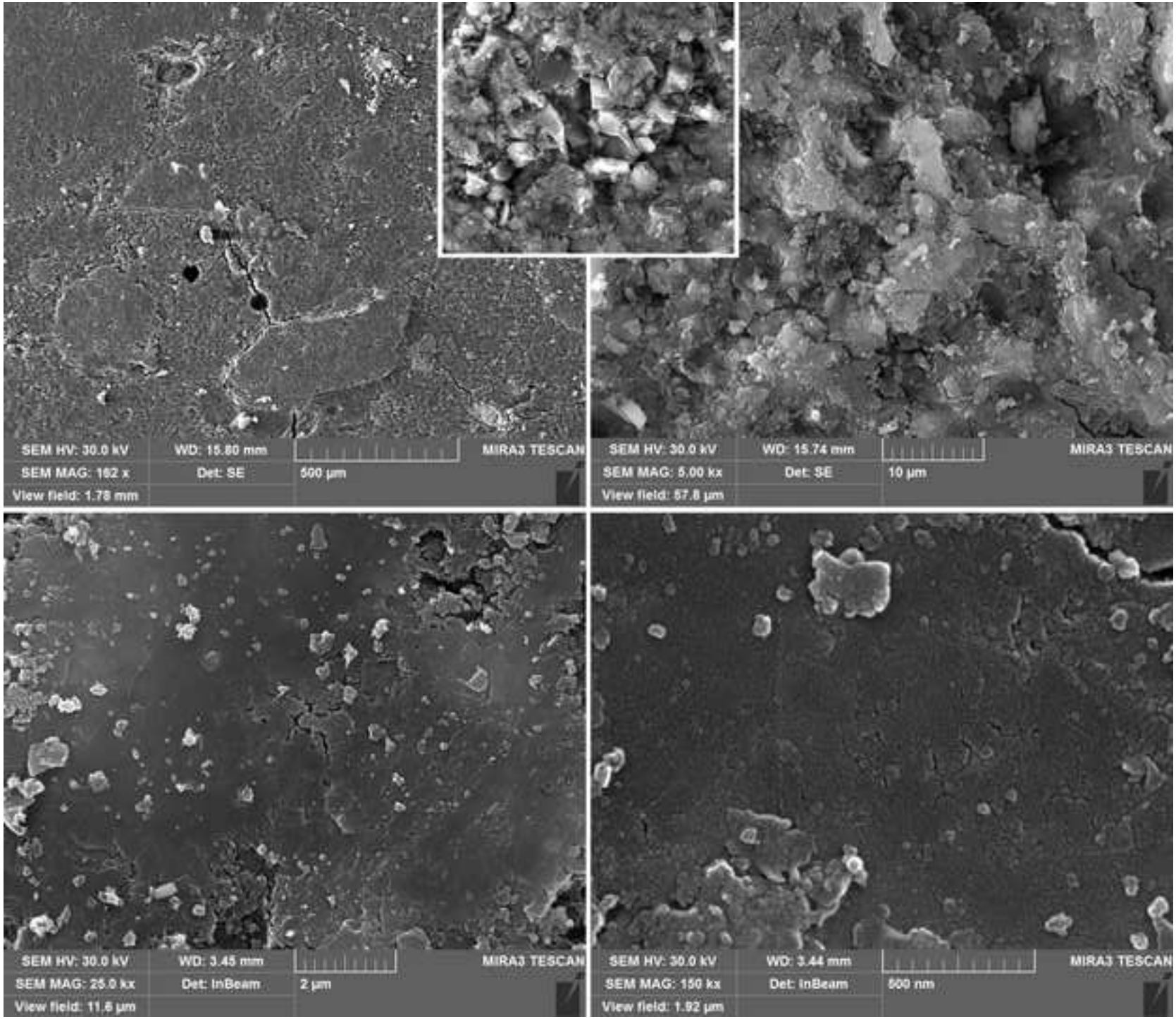

Figure 7

Click here to download high resolution image

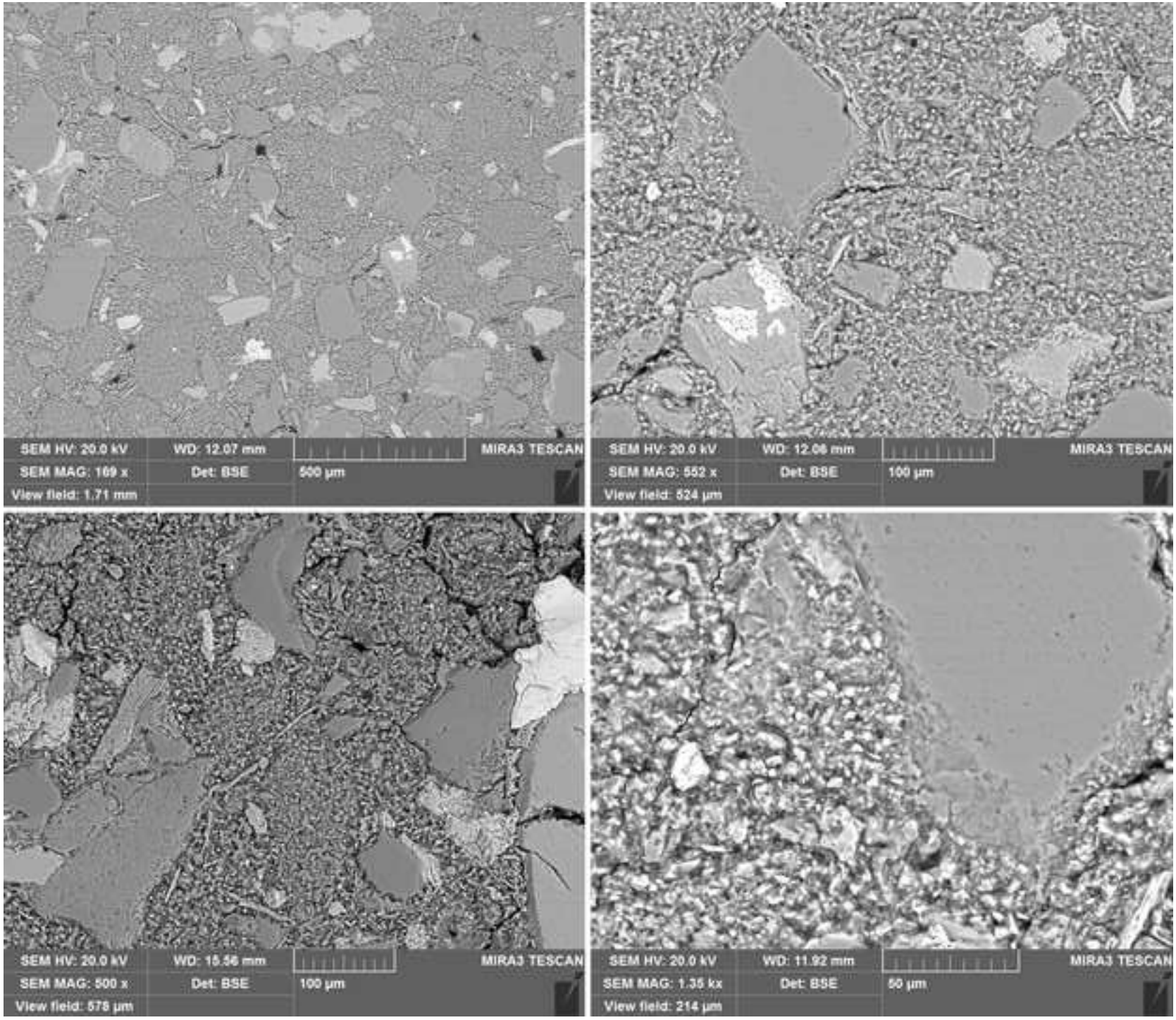

Figure 8

Click here to download high resolution image